Universality in the Morphology and Mechanics of Coarsening Amyloid Fibril Networks

L. G. Rizzi,[1] D. A. Head,[2] and S. Auer[1]
[1]School of Chemistry, University of Leeds, LS2 9JT Leeds, United Kingdom
[2]School of Computing, University of Leeds, LS2 9JT Leeds, United Kingdom
(Received 22 May 2014; published 18 February 2015)

Peptide hydrogels have important applications as biomaterials and in nanotechnology, but utilization often depends on their mechanical properties for which we currently have no predictive capability. Here we use a peptide model to simulate the formation of percolating amyloid fibril networks and couple these to the elastic network theory to determine their mechanical properties. We find that the time variation of network length scales can be collapsed onto master curves by using a time scaling function that depends on the peptide interaction anisotropy. The same scaling applies to network mechanics, revealing a nonmonotonic dependence of the shear modulus with time. Our structure-function relationship between the peptide building blocks, network morphology, and network mechanical properties can aid in the design of amyloid fibril networks with tailored mechanical properties.

DOI: 10.1103/PhysRevLett.114.078102 PACS numbers: 87.14.em, 87.10.Hk, 87.10.Pq, 89.75.Da

Amyloid fibril networks form via two stages. First, peptides or proteins assemble into amyloid fibrils that share a common cross-β structure of intertwined layers of β sheets extending in a direction parallel to the fibril axis [1,2]. Fibril lengthening and thickening can be attributed to strongly directional backbone hydrogen bonding and weaker side-chain interactions, respectively. At later times, the amyloid fibrils may entangle into a percolating network [3] with a morphology characterized by multiple length scales. Although amyloid fibrils are often associated with devastating diseases such as Alzheimer's and Parkinson's [4], amyloid networks are emerging as an important class of material with applications in biosensing, nanoelectronics, tissue engineering, and drug delivery [5–7]. However, many of these applications depend strongly on the network's mechanical properties, for which we currently have no predictive structure-function relation between the bulk network stiffness and the properties of individual proteins, without making assumptions regarding the fibril morphology, cross-linker dynamics, and the local deformation regime.

Theoretical and experimental studies characterizing the mechanical properties of single, isolated amyloid fibrils show that their elastic modulus and bending stiffness are comparable to semiflexible filaments like actin, keratin, collagen, and spider silk [8–11]. Recent rheology experiments demonstrate that the shear modulus of amyloid fibril networks can be altered by changes in the amino acid sequence of the peptides [12,13] and the ionic strength of the solution [14–17], indicating that design principles might exist. The viscoelastic response of semiflexible polymer networks can be immediately related to the properties of individual filaments under the assumption of affinity, i.e., that the microscopic deformation field follows the applied macroscopic strain [18–22]. Relaxing this assumption has thus far been possible only for the zero-frequency response of athermal networks, formally corresponding to the elastic plateau where the cross-links can be regarded as fixed [23–25]. Importantly, all of the mentioned theoretical approaches assume that the filaments are identical, having the same bending rigidity, or, equivalently, persistence length, at every location. This is a valid assumption for filaments such as actin but not for amyloid fibrils where the fibril thickness varies throughout the network [26–28]. Furthermore, these previous studies considered procedurally defined, static networks; the time evolution of the network morphology was not considered. The objective of this Letter is to model the formation of amyloid fibril networks to determine their mechanical properties without making the aforementioned assumptions.

Our simulations use a peptide model similar to those used in recent studies on amyloid fibril aggregation [29–32], where the peptides in their virtually fully extended (β-strand) conformation are described as hexagons positioned on a two-dimensional (2D) triangular lattice that assemble into a cross-β structure characteristic of amyloids [see Fig. S1(a) in Supplemental Material [33]]. The use of a triangular lattice ensures that the network's mechanical properties are isotropic at large length scales [37], as well as enabling the correct stacking of β sheets in fibrils [38] [see Fig. S1(b) in Supplemental Material]. The hexagon has two opposing strong bonding sides that allow the formation of directional backbone hydrogen bonds, with the remaining four weak bonding sides controlling fibril thickening. The strong and weak bond energies are denoted $\psi = E/k_BT$ and $\psi_h = E_h/k_BT$, respectively, where k_B is Boltzmann's constant and T temperature. The cross-β structure so formed reproduces key aspects of the atomic structure of fibrils formed by, e.g., the TTR peptide [2], and the structure of fibrils formed by short segments of insulin

observed in microcrystals [39]. Here we fix $\psi_h = 1$ while varying ψ, to study effect of the ratio $\xi = \psi/\psi_h$ of the hydrogen bond energy to the side-chain bond energy. A value of $\xi = 14$ has been estimated for the $A\beta_{40}$ peptide [31].

In order to model the formation of amyloid fibril networks, we perform Monte Carlo (MC) simulations similar to those described in Ref. [29]. We perform displacement moves of peptides to nearest neighbor lattice sites and rotation moves so that the peptide can change its orientation. At the beginning of a simulation, N peptides are randomly placed and oriented on a periodic 2D triangular lattice of linear size L. In all our simulations, we set $L = 256$. As we use only physically plausible moves, our model peptides exhibit the layer by layer growth mechanism observed in computer simulations of the self-assembly of short peptides into fibrillar aggregates [40,41], and there is a correspondence between the number of MC steps (MCSs) and real time as suggested in Refs. [29,32,42]. A typical configuration is shown in Fig. 1(a). The morphology of the fibril network obtained is very similar to those observed experimentally for $A\beta$25-35 [43] and short synthetic peptides (e.g., for GAV-9 [44]). We use the Hoshen-Kopelman algorithm [45] to identify individual amyloid fibrils, which enable us to characterize them by their thickness i and length m [see Fig. S1(b) in Supplemental Material]. The identification of fibrils also allows us to obtain an elastic network representation of the system as shown in Fig. 1(b). The cross-link positions are taken to be the geometric centers of the overlap region between different fibrils (see Fig. S2 in Supplemental Material), with the distance between two connected cross-links defined as the cross-link length l. Note that not all fibrils identified in the system are part of the percolating network [Fig. 1(a)].

The time evolution of the mean fibril thickness $\langle i \rangle$, the mean cross-link distance $\langle l \rangle$, and the mean fibril length $\langle m \rangle$ is shown in Fig. 2 for anisotropy ratios $\xi = 7$, 10, and 14, at a coverage $\theta = N/L^2 = 0.5$. As can be seen in the insets in this figure, all lengths enter a coarsening regime where they monotonically increase; i.e., the fibrils become thicker and longer, and the cross-link positions become further apart as the network evolves. Increasing the anisotropy ratio ξ delays the onset of coarsening. A similar effect, where the dynamics of the system is slowed down due to stronger effective interparticle interactions, has been observed in colloidal gels and glasses [46,47]. As demonstrated in Fig. 2, the time dependence of each morphological quantity of the network obtained for different anisotropy ratios can be collapsed onto a single master curve by rescaling the time as $t_\xi = te^{-\Delta\xi}$, where $\Delta\xi = \xi - \xi_0$ with ξ_0 an arbitrary origin (here we take $\xi_0 = 7$). It is not only the mean of the morphological quantities that collapse, but also their distribution functions as shown in Fig. S3 in Supplemental Material. The coarsening exponents $\alpha_i = 0.16 \pm 0.02$, $\alpha_l = 0.18 \pm 0.02$, and $\alpha_m = 0.17 \pm 0.02$ of the morphological quantities can be obtained by fitting the data points for times $\ln(t_\xi) > 6$ to $\langle i \rangle \sim t_\xi^{\alpha_i}$, $\langle l \rangle \sim t_\xi^{\alpha_l}$, and $\langle m_\xi \rangle \sim t_\xi^{\alpha_m}$, respectively. The mean fibril length was additionally scaled by an arbitrary function $w(\xi)$ [inset in Fig. 2(c)], giving $\langle m_\xi \rangle = \langle m \rangle e^{w(\xi)}$, but this does not affect the scaling with time. The measured exponents are consistent with a common value ≈ 0.17, demonstrating that all network lengths obey the same scaling during coarsening. Note that, if one identifies the fibril area $s \approx i \times m$ as a domain size, the growth law $s \sim t_\xi^{\alpha_i + \alpha_m}$ is consistent with the $1/3$ exponent derived analytically for the isotropic case, i.e., the 2D spin-exchange Ising model [48,49], despite the fibrils in our networks forming anisotropic shapes.

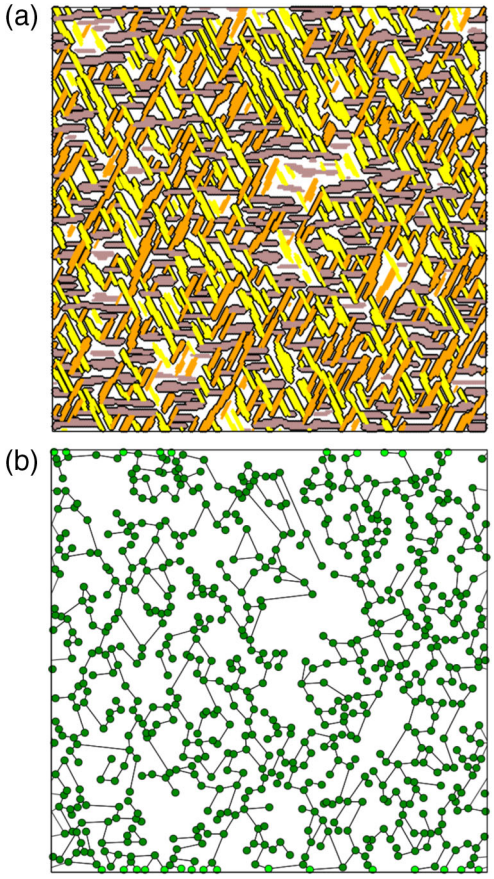

FIG. 1 (color online). (a) Amyloid fibril network obtained for $\xi = 10$ with $N = 31130$ peptides on a 2D lattice with linear size $L = 256$ at time $t = 10^5$ MC steps. Fibrils that are part of the percolation network are shown with a black border. The three possible orientations of the fibril on the triangular lattice are distinguished by three different colors/shades. (b) Corresponding elastic network representation where fibril cross-links are represented by circles and the fibrils between cross-links by line segments.

We now turn our attention to understanding how the structural changes in the network affect its mechanical properties. Starting from the network representation as in

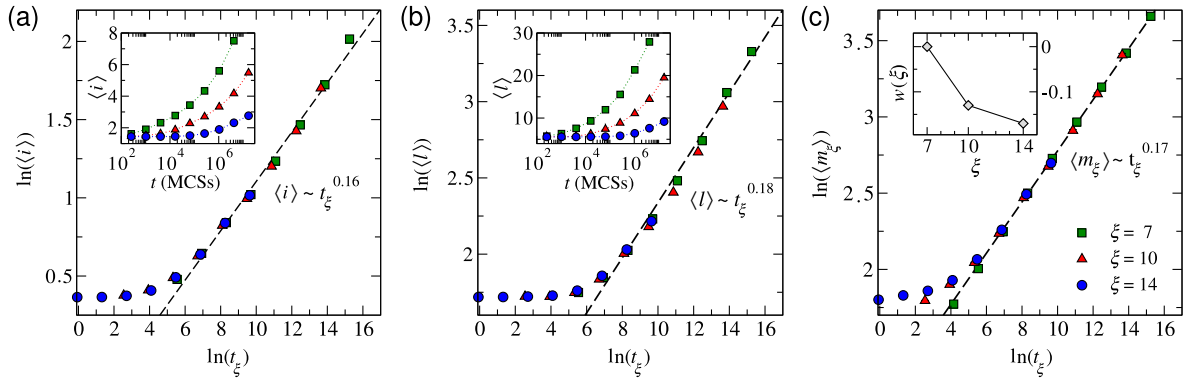

FIG. 2 (color online). (a) Scaled and unscaled (inset) time dependence of the mean thickness $\langle i \rangle$. (b) Scaled and unscaled (inset) time dependence of mean cross-link length $\langle l \rangle$. (c) Scaled time dependence of mean fibril length $\langle m_\xi \rangle = \langle m \rangle e^{w(\xi)}$, where the values of the function $w(\xi)$ used are shown in the inset. The data are obtained from configurations for a coverage $\theta = 0.5$ at times $t = 4^n$ MCSs, with $n = 1, 2, \ldots, 12$. Averages were obtained from 25 independent simulations. Error bars are smaller than the symbols. Dashed lines are fits for $\ln(t_\xi) > 6$ as discussed in the text.

Fig. 1(b), one can mimic an applied strain γ by imposing horizontal displacements to the boundary cross-links as shown in Fig. S4 in Supplemental Material. The internal cross-links then relax to new positions, causing an increase $\Delta E_{\text{elastic}}$ in the total elastic energy of the network. For the linear response ($\gamma \ll 1$), one can use $\Delta E_{\text{elastic}}$ to extract the shear modulus [25,37]:

$$G = \frac{2\Delta E_{\text{elastic}}}{\gamma^2 A}, \tag{1}$$

where A is the total system area. The shear modulus G thus depends on the displacement vectors $\vec{u}_\nu$ of all cross-links, which contribute to $\Delta E_{\text{elastic}}$ as detailed in Supplemental Material. These displacement vectors $\vec{u}_\nu$ are obtained by performing high-dimensional numerical optimization to minimize $\Delta E_{\text{elastic}}$ with respect to each displacement degree of freedom [23]. For all measurements we consider $\gamma = 0.02$ to avoid nonlinear responses due to high strain values. Our method generalizes a previous lattice-based model [25] by permitting variations in fibril thickness and cross-link distances (see Supplemental Material).

In Fig. 3, we present results for the time-dependent behavior of the normalized shear modulus G/E^f, where E^f is the Young's modulus of a fibril. It is evident that small changes in both the anisotropy ξ and the coverage θ lead to large changes in G spanning orders of magnitude, with an overall trend for higher values of G/E^f with increasing θ. Moreover, the variation is nonmonotonic in time, in contrast to the monotonic coarsening of the morphological quantities discussed above, and there are time periods when the thinner fibrils (formed for $\xi = 14$) yield stronger networks than thicker fibrils. Most experiments on the formation of amyloid fibril networks are performed on a time scale of tens of minutes, where the shear modulus displays either an increasing or a constant behavior [14,16,50,51]. However, one set of longer experiments for β-lactoglobulin gels suggested a slight decrease in G after hours [52], and atomic force microscopy imaging has demonstrated significant changes to network morphology over a time scale of days [43,53], for which mechanical properties are not usually measured. This suggests that extending the data acquisition window may reveal a similar nonmonotonicity to Fig. 3. Although we simulate a 2D network, a rough estimate for the shear modulus G_{exp} as measured in 3D experiments can be made by scaling our results by $G^{\text{aff}}_{\text{3D}}/G^{\text{aff}}_{\text{2D}}$, where $G^{\text{aff}}_{\text{2D}}$ and $G^{\text{aff}}_{\text{3D}}$ are the affine predictions in 2D and 3D, respectively. By employing standard results [23,25], $G_{\text{exp}} = (8E^f/15\ell_c)(G/E^f)$ for tightly entangled networks, where ℓ_c is a length scale comparable to the cross-link distance $\langle l \rangle$. Taking the Young's modulus of a single fibril to be $E^f \sim 10^9$ Pa [10] and $\ell_c \sim 10$ nm, we obtain values for G_{exp} spanning

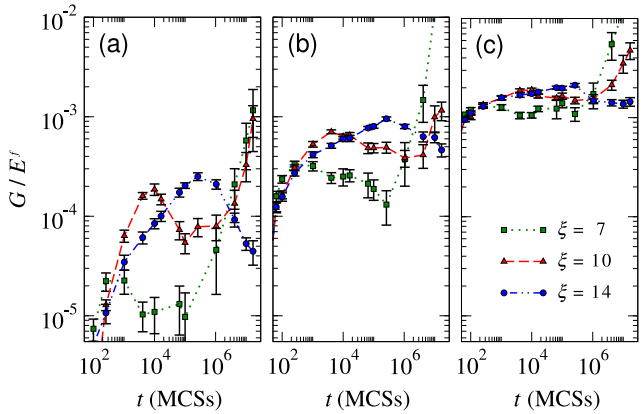

FIG. 3 (color online). Time dependence of the normalized shear modulus G/E^f obtained for networks with coverages (a) $\theta = 0.5$, (b) 0.525, and (c) 0.55. Averages and errors bars were obtained from 25 independent simulations. Additional points at times $t = 10^n$ ($n \in \mathbb{N}$) are also included.

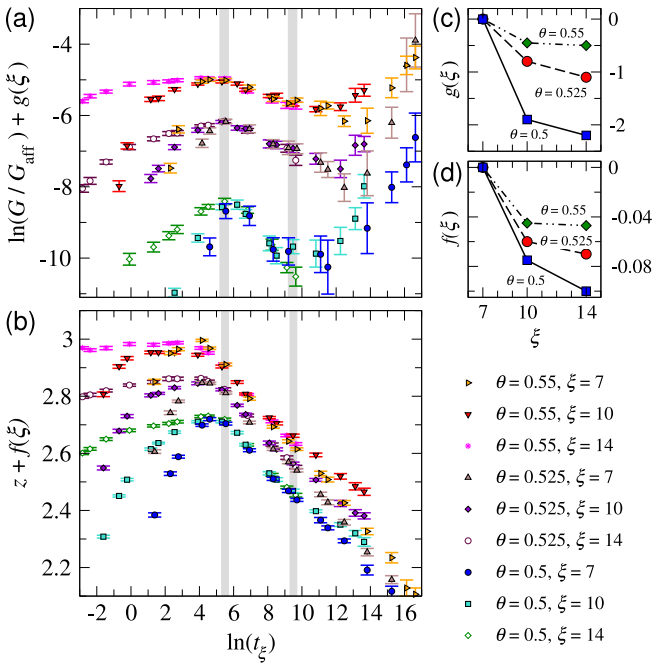

FIG. 4 (color online). Scaling behavior of (a) shear modulus ratio G/G_{aff} and (b) mean network connectivity z against the rescaled time t_ξ. Data collapse is obtained separately for each coverage θ. Vertical gray bars denote regions near the maximum and minimum of G/E^f. (c) and (d) show the values of the scaling functions $g(\xi)$ and $f(\xi)$ for the shear modulus ratio and connectivity, respectively.

10^2–10^4 Pa, which is the same range observed for β-lactoglobulin gels [52] and other peptide-based gels (e.g., Refs. [17,51]). In addition, the behavior of G/E^f resembles that of weakly interacting colloidal aggregates which measurably weaken prior to visual collapse [54]. We hypothesize that this weakening shares a common mechanism to that observed in our results, although the final collapse under gravity (with its associated step change in the bulk symmetry) presumably has a different origin.

Insight into the mechanism underlying network weakening can be gained by measuring mechanical and morphological quantities simultaneously. We evaluated the shear modulus normalized to the affine prediction G_{aff} [computed from Eq. (1) for identical networks with affine displacements $\vec{u}_\nu^{\text{aff}}$] as in previous works [23,25] and monitored the mean network connectivity z given by the average value of the coordination numbers, z_ν, from all internal cross-links. As depicted in Fig. 4(a), we found that G/G_{aff} for different anisotropies ξ can be collapsed onto a series of master curves, with one such curve for each coverage θ. The decreasing region of G/G_{aff} coincides with the onset of a decrease in z as indicated in the diagram, and indeed snapshots reveal a reduction in network connectivity over these times (see Fig. S5 in Supplemental Material). Thus, the mechanical weakening of the network is due to its increased sparsity. As with the fibril length $\langle m_\xi \rangle$, it was also necessary to scale the magnitude of G/G_{aff} by ξ-dependent factors $f(\xi)$ and $g(\xi)$ as shown in Figs. 4(c) and 4(d), but this does not alter the times t_ξ corresponding to the local minimum and maximum in G/G_{aff}. These factors mean that, at fixed rescaled times t_ξ, higher ξ yields higher G/G_{aff} and correspondingly higher values of z. For all values of θ and ξ, the values of z are located below the central force threshold ($z_{\text{CF}} = 4$ for 2D systems). Moreover, we find $G/G_{\text{aff}} \ll 1$ for our networks, as evident in Fig. 4(a). Thus all of our networks correspond to a nonaffine deformation regime, and consistent with prior observations [25] most of the elastic energy takes the form of fibril bending, with $\Delta E_{\text{bending}}/\Delta E_{\text{elastic}}$ fluctuating around 0.9 (see Fig. S6 in Supplemental Material).

Identifying universal behaviors, such as in time-cure superposition curves [52,55], can accelerate the development of novel materials by reducing the number of independent parameters that need to be assayed. Our simulations have revealed a simple time scaling function that depends on the anisotropy ξ of interaction between peptides, which collapses data for both morphological and mechanical quantities. The proposed scaling function should benefit experimentalists in the design of amyloid-based materials, since it permits the extrapolation of the time-dependent mechanical response of the amyloid fibril networks from the behavior of peptide systems with known interactions. Our findings indicate that features like the nonzero shear modulus for connectivities lower than z_{CF} and the nonaffine response, which are commonly overlooked in the modeling of hydrogels [21,22], should be included in further descriptions of amyloid fibril networks. Finally, we note that our hybrid approach to measure the elastic moduli of a fiber network as it forms and grows represents a new direction for fiber network modeling that can be extended to other fibrous and porous materials in general, including inorganic materials such as colloidal gels [46].

L. G. R. acknowledges support from the Brazilian agency Conselho Nacional de Desenvolvimento Científico e Tecnológico (CNPq) (Grant No. 245412/2012-3). D. A. H. acknowledges support from the Biomedical Health Research Centre, University of Leeds, United Kingdom.

[1] J. Adamcik and R. Mezzenga, Macromolecules **45**, 1137 (2012).
[2] A. W. P. Fitzpatrick, G. T. Debelouchina, M. J. Bayro, D. K. Claire, M. A. Caporini, W. S. Bajaj, C. P. Jaroniec, L. Wang, V. Ladizhansky, S. A. Müller, C. E. MacPhee, C. A. Wauldby, H. R. Mott, A. D. Simone, T. P. J. Knowles, H. R. Saibil, M. Vendruscolo, E. V. Orlova, R. G. Griffin, and C. M. Dobson, Proc. Natl. Acad. Sci. U.S.A. **110**, 5468 (2013).

[3] M. Schleegert, C. C. vanderAkker, T. Deckert-Gaudig, V. Deckert, K. P. Velikov, G. Koenderink, and M. Bonn, Polymer **54**, 2473 (2013).
[4] F. Chiti and C. M. Dobson, Annu. Rev. Biochem. **75**, 333 (2006).
[5] I. Cherny and E. Gazit, Angew. Chem., Int. Ed. **47**, 4062 (2008).
[6] C. J. Bowerman and B. L. Nilsson, Biopolymers **98**, 169 (2012).
[7] N. P. Reynolds, M. Charnley, R. Mezzenga, and P. G. Hartley, Biomacromolecules **15**, 599 (2014).
[8] J. F. Smith, T. P. J. Knowles, C. M. Dobson, C. E. MacPhee, and M. Welland, Proc. Natl. Acad. Sci. U.S.A. **103**, 15806 (2006).
[9] T. P. J. Knowles and M. J. Buehler, Nat. Nanotechnol. **6**, 469 (2011).
[10] L. R. Volpatti and T. P. J. Knowles, J. Polym. Sci. B **52**, 281 (2014).
[11] S. Keten, Z. Xu, B. Ihle, and M. J. Buehler, Nat. Mater. **9**, 359 (2010).
[12] C. Tang, R. Ulijn, and A. Saiani, Langmuir **27**, 14438 (2011).
[13] J. Adler, H. A. Scheidt, M. Krüger, L. Thomas, and D. Huster, Phys. Chem. Chem. Phys. **16**, 7461 (2014).
[14] B. B. Ozbas, K. K. Rajagopal, J. P. J. Schneider, and D. J. Pochan, Macromolecules **37**, 7331 (2004).
[15] J. M. Riley, A. Aggeli, R. J. Koopmans, and M. J. McPherson, Biotechnol. Bioeng. **103**, 241 (2009).
[16] S. Bolisetty, L. Harnau, J.-M. Jung, and R. Mezzenga, Biomacromolecules **13**, 3241 (2012).
[17] S. Boothroyd, A. F. Miller, and A. Saiani, Faraday Discuss. **166**, 195 (2013).
[18] R. Pritchard, Y. Y. S. Huang, and E. M. Terentjev, Soft Matter **10**, 1864 (2014).
[19] C. P. Broedersz, M. Depken, N. Y. Yao, M. R. Pollak, D. A. Weitz, and F. C. MacKintosh, Phys. Rev. Lett. **105**, 238101 (2010).
[20] L. Wolff, P. Fernandez, and K. Kroy, New J. Phys. **12**, 053024 (2010).
[21] A. Basu, Q. Wen, X. Mao, T. C. Lubensky, P. A. Janmey, and A. G. Yodh, Macromolecules **44**, 1671 (2011).
[22] Q. Wen, A. Basu, P. A. Janmey, and A. G. Yodhb, Soft Matter **8**, 8039 (2012).
[23] D. A. Head, A. Levine, and F. MacKintosh, Phys. Rev. Lett. **91**, 108102 (2003); Phys. Rev. E **68**, 061907 (2003).
[24] C. Heussinger and E. Frey, Phys. Rev. Lett. **97**, 105501 (2006).
[25] C. P. Broedersz, X. Mao, T. C. Lubensky, and F. C. MacKintosh, Nat. Phys. **7**, 983 (2011).
[26] M. Kolsofszki, A. Karsai, K. Soós, B. Penke, and M. S. Z. Kellermayer, Prog. Colloid Polym. Sci. **135**, 169 (2008).
[27] W. F. Xue, S. W. Homans, and S. E. Radford, Protein Eng., Des. Sel. **22**, 489 (2009).
[28] R. J. Morris, K. Eden, R. Yarwood, L. Jourdain, R. J. Allen, and C. E. MacPhee, Nat. Commun. **4**, 1891 (2013).
[29] J. Zhang and M. Muthukumar, J. Chem. Phys. **130**, 035102 (2009).
[30] R. Cabriolu, D. Kashchiev, and S. Auer, J. Chem. Phys. **137**, 204903 (2012).
[31] D. Kashchiev, R. Cabriolu, and S. Auer, J. Am. Chem. Soc. **135**, 1531 (2013).
[32] A. Irback, S. Jonsson, N. Linnemann, B. Linse, and S. Wallin, Phys. Rev. Lett. **110**, 058101 (2013).
[33] See Supplemental Material at http://link.aps.org/supplemental/10.1103/PhysRevLett.114.078102 for detailed methodology, further snapshots and additional results, which includes Refs. [34–36].
[34] M. Bathe, C. Heussinger, M. M. A. E. Claessens, A. R. Bausch, and E. Frey, Biophys. J. **94**, 2955 (2008).
[35] P. Müller and J. Kierfeld, Phys. Rev. Lett. **112**, 094303 (2014).
[36] T. Boatwright, A. J. Levine, and M. Dennin, Soft Matter **7**, 7851 (2011).
[37] L. D. Landau and E. M. Lifshitz, *Theory of Elasticity* (Butterworth-Heinemann, Oxford, 1986).
[38] H. D. Nguyen and C. K. Hall, J. Biol. Chem. **280**, 9074 (2005).
[39] M. R. Sawaya, S. Sambashivan, R. Nelson, M. I. Ivanova, S. A. Sievers, M. I. Apostol, M. J. Thompson, M. Balbirnie, J. J. W. Wiltzius, H. T. McFarlane, A. Madsen, C. Riekel, and D. Eisenberg, Nature (London) **447**, 453 (2007).
[40] S. Auer and D. Kashchiev, Phys. Rev. Lett. **104**, 168105 (2010).
[41] M. Cheon, I. Chang, and C. K. Hall, Biophys. J. **101**, 2493 (2011).
[42] B. Linse and S. Linse, Mol. Biosyst. **7**, 2296 (2011).
[43] A. Karsai, L. Grama, U. Murvai, K. Soos, B. Penke, and M. S. Z. Hellermayer, Nanotechnology **18**, 345102 (2007).
[44] H. Li, F. Zhang, Y. Zhang, M. Ye, B. Zhou, Y.-Z. Tang, H.-J. Yang, M.-Y. Xie, S.-F. Chen, J.-H. He, H.-P. Fang, and J. Hu, J. Phys. Chem. B **113**, 8795 (2009).
[45] J. Hoshen and R. Kopelman, Phys. Rev. B **14**, 3438 (1976).
[46] P. J. Lu and D. A. Weitz, Annu. Rev. Condens. Matter Phys. **4**, 217 (2013).
[47] G. L. Hunter and E. R. Weeks, Rep. Prog. Phys. **75**, 066501 (2012).
[48] J. G. Amar, F. E. Sullivan, and R. D. Mountain, Phys. Rev. B **37**, 196 (1988).
[49] S. J. Mitchell and D. P. Landau, Phys. Rev. Lett. **97**, 025701 (2006).
[50] A. Aggeli, M. Bell, N. Boden, J. N. Keen, P. F. Knowles, T. C. B. McLeish, M. Pitkeath, and S. E. Radford, Nature (London) **386**, 259 (1997).
[51] M. A. Greenfield, J. R. Hoffman, M. O. de la Cruz, and S. I. Stupp, Langmuir **26**, 3641 (2010).
[52] W. S. Gosal, A. H. Clark, and S. B. Ross-Murphy, Biomacromolecules **5**, 2420 (2004).
[53] I. Usov, J. Adamcik, and R. Mezzenga, Faraday Discuss. **166**, 151 (2013).
[54] S. W. Kamp and M. L. Kilfoil, Soft Matter **5**, 2438 (2009).
[55] A. M. Corrigan and A. M. Donald, Eur. Phys. J. E **28**, 457 (2009); Langmuir **25**, 8599 (2009).